

Fuel-Powered Compact SMA Actuator

Othon K. Rediniotis^a, Dimitris C. Lagoudas^a, Hyoung Y. Jun^a, Richard D. Allen^a

Aerospace Engineering Department
Texas A&M University, College Station, TX 77843-3141

ABSTRACT

This work discusses the numerical analysis, the design and experimental test of the fuel-powered compact SMA actuator along with its capabilities and limitations. Convection heating and cooling using water actuate the SMA element of the actuator. The energy of fuels, having a high energy density, is used as the energy source for the SMA actuator in order to increase power and energy density of the system, and thus in order to obviate the need for electrical power supplies such as batteries. The system is composed of pump, valves, bellows, heater (burner), control unit and a displacement amplification device. The experimental test of the first designed SMA actuator system results in 150 MPa stress (force: 1560N) with 3 % strain and 0.5 Hz actuation frequency. The actuation frequency is compared with the prediction obtained from numerical analysis. For the first designed fuel-powered SMA actuator system, the results of numerical analysis were utilized in determining design parameters and operating conditions.

Keywords: Shape Memory Alloys (SMA), actuator, convection heat transfer, efficiency, fuel, power density, energy density.

1. INTRODUCTION

The main objective of this research is to design, fabricate and test a highly compact shape memory alloy based actuator that utilizes the high energy density of fuels, such as propane. The fact that the main element of the actuator, the SMA is a heat engine [1][2][3], is used to convert the thermal energy of a fuel (propane) to mechanical energy. The high energy density of fuels compared to typical electrical batteries, or even fuel cells, allows for the energy source, i.e. the fuel, to be incorporated inside the actuator system. The energy density (J/kg) of these fuels is 100 times greater than that of most advanced batteries. This, along with the incorporation of the actuation control hardware and software inside the unit, can result in a highly compact actuator. Thus the actuator system can be run wirelessly by low-power, digital, actuator control signals. The high-energy density, high recovery stress and strain of SMA will result in high actuator compactness, force and stroke, respectively.

The phase change in a NiTi SMA is achieved by heat exchange with a heat source and a heat sink. The actuation frequency of the SMA actuator is only dependent on the rate of heat transfer with its surroundings. Until recently, the heat transfer mechanism for most SMA actuators has been based on resistive heating ($M \rightarrow A$) and cooling with forced convection or natural convection ($M \rightarrow A$). This is a rather inefficient heat exchange mechanism [4] and requires the use of electrical power and thus heavy, low-energy-density (at least as compared to fuels) power supplies or batteries. The thermoelectric heat transfer mechanism by utilizing semiconductors, which employing the Peltier effect, has shown high actuation frequency [5]. But generally this kind of device has very low efficiency. Thus, we propose forced convection heating and cooling to actuate the SMA actuator. This can overcome the low energy density resistive heating systems and the low efficiency of the thermoelectric heat transfer mechanism, even though it should need additional devices such as a pump and valves. Also, the high energy of fuel is transferred easily to the fluid through the combustor and the heat exchanger. Researchers have worked on developing high efficiency, compact combustors and heat exchangers, using micro technology [6][7]. Convection heating and cooling of the SMA, can result in considerable actuation frequencies. In addition, for systems with sufficient parasitic heat, the actuator can utilize the parasitic heat as its energy source, resulting in a relatively high-efficiency actuating system. The actuator design merges the advantages of SMAs and fuels, i.e., the high actuation forces, the large power densities and the silent actuation characteristics of SMAs and the

^a Further Author information (Send correspondence to O.K.R)

O.K.R: email: rediniotis@aero.tamu.edu, D.C.L: email: lagoudas@aero.tamu.edu,

H.Y.J: email: hyoungyoll@aero.tamu.edu, R.D.A: email : minitman@aero.tamu.edu

tremendous energy densities of fuels. In this paper we will discuss the design of the SMA actuator system, recovery stress and strain and actuation frequency of the SMA actuator by utilizing the high thermal energy of fuels. Section 2 of this paper presents the principle of the fuel-powered compact SMA actuator system, comparison with other actuator systems and thermal & Carnot efficiencies of the SMA element of the actuator. Section 3 presents the numerical heat transfer analysis of the SMA actuator. Section 4 is for the first design of the fuel-powered SMA actuator system and its components. Section 5 presents experimental results and comparison with numerical results and discusses the system’s capabilities and limitations.

2. DESIGN CONCEPT AND EFFICIENCY OF THE SMA ACTUTATOR SYSTEM

2.1 Energy Density and Power Density

The following data describes the design parameters of the SMA element of actuator systems of figure 1. This data can be modified accordingly to meet different requirements for the actuator. A NiTi SMA strip with a rectangular cross section measuring about 12 mm x 1 mm (12 mm² cross sectional area) was selected as the SMA element to increase heat transfer rate compared to a wire having the same cross section area. Four such strips can be installed in a rectangular channel with 12 mm x 16 mm cross section. Our work, [8][9][10], during the last several years has lead to precise actuation control techniques for NiTi SMAs at stress levels of 200 M Pa and actuation strains of 3 %. These numbers are used here in our design. In order for the SMA strip to produce bi-directional loads it will have to be pre-stressed. This could be achieved as easily as via a stress-biasing spring. If, for example, a stress bias level of 100M Pa is chosen, the SMA strip will be able to produce bi-directional actuation loads at the level of $\pm(100 \text{ M pa}) \times (\text{strip cross sectional area})$, or, $\pm 1,200 \text{ N}$ (or 2,400 N uni-directional). An arrangement of four such strips in an array will yield a combined bi-directional actuation force of $\pm 4,800 \text{ N}$. For a SMA strip length of 254 mm the SMA actuation stroke (at 3 % strain) is 7.62 mm (0.76 cm).

The first system in figure 1 referred to as the SMA-Combustor system, comprises of two pumps, a combustor, the SMA element, the cooling circuit heat exchanger and fuel as energy source. The SMA strips are embedded in a channel. Heating and cooling fluid medium alternatively circulates through the channel to achieve the M-to-A and A-to-M transformations, respectively. The heating medium (Ethylene Glycol or water) is heated through the burning of the fuel in the combustor. The cooling medium, after it removes the heat from the SMAs goes through a heat exchanger where it dispose of the energy getting from the SMA strips. The two pumps that circulate the two media are equipped with valves that are properly timed through the heating and cooling cycles.

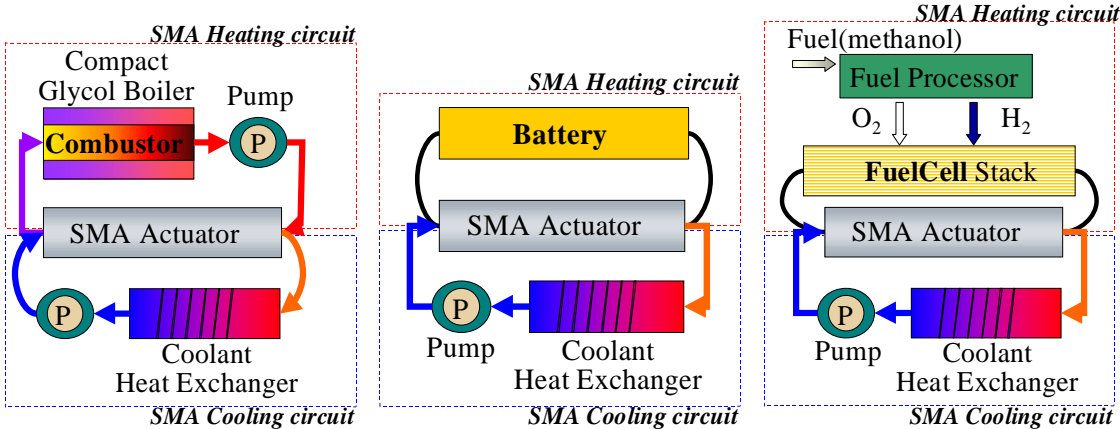


Figure 1. Compact Actuator Systems with fuel+combustor, battery and fuelcell as energy source.

Alternative energy sources like batteries and fuel cells have been considered as energy sources for the SMA actuator in the other two systems of figure 1. The results of the comparison have been tabulated in tables 1 and 2 for different cases of actuation cycle number (1000, 10000, 100000 actuation cycles). These tables show that the SMA-Combustor compact actuator has high energy and power densities compared to battery and fuel cell powered systems. The fuel cell stack itself has high energy and power densities, but needs additional equipment such as a reformer or a hydrogen tank, a cleanup unit, a bower, a compressor and cooling devices [11][12], especially for a large number of actuation cycles. The main disadvantage of the fuel cell system is the large mass of the fuel processing unit or the mass of the fuel tank. All these factors combined give a low energy/power density for the SMA-Fuel Cell actuator system. In the case of a battery powered SMA (SMA-Battery) actuator system, the mass of the battery increases significantly with the increase in number of actuation cycles even having the highest efficiency: this, coupled with the fact that batteries have low energy densities compared to fuel cells or fuels [13][14], yields the lowest overall energy/power densities for this system.

Table 1. Output Energy Density (Total Mechanical Work/Mass of System).

Actuator Systems	1,000 Cycle	10,000 Cycle	100,000 Cycle
SMA-Combustor	9.887(Wh/kg)	71.04(Wh/kg)	193.6(Wh/kg)
SMA-Battery	3.717(Wh/kg)	4.411(Wh/kg)	4.495(Wh/kg)
SMA-Fuel Cell	0.7605(Wh/kg)	7.038(Wh/kg)	41.1(Wh/kg)

Table 2. Output Power Density (Total Mechanical Work/(Mass of System × Cycle)).

Actuator Systems	1,000 Cycle	10,000 Cycle	100,000 Cycle
SMA-Combustor	35.59(W/kg)	25.57(W/kg)	6.971(W/kg)
SMA-Battery	13.38(W/kg)	1.588(W/kg)	0.1618(W/kg)
SMA-Fuel Cell	2.738(W/kg)	2.534(W/kg)	1.48(W/kg)

Table 3. Efficiency of the system

Actuator Systems	1,000 Cycle	10,000 Cycle	100,000 Cycle
SMA-Combustor	2.253(%)	2.318(%)	2.325(%)
SMA-Battery	2.999(%)	3.003(%)	3.003(%)
SMA-Fuel Cell	2.499(%)	2.502(%)	2.503(%)

2.2 Efficiency

In the design and development of SMA actuators, the available thermal efficiency and their limits must be calculated and considered. Lagoudas and Bhattacharyya [15] evaluated the efficiency of the thermoelectric SMA actuators. Jardine[16] and Gil [17] proposed the calorimetric techniques and mechanical tests to evaluate the efficiency of shape memory alloys based on ideal shape memory effect (SME) heat engine cycle[18].

Transformation temperatures of an SMA strip (DSC test)

The phase transformation temperatures and latent heat were first determined in order to calculate the thermal efficiency of SMA strip. The strip utilized in this study was provided by Memory Corporation and is a Copper 10 % NiTi alloy. A Perkin-Elmer Pyris 1 Differential Scanning Calorimeter (DSC) was used to determine the phase transformation temperatures and heat of transformation. ΔH is measured as the total area under the curve during the heating and cooling cycle. The cooling cycle was started after holding for 1.0 minute at 120 °C. The SMA was then cooled from 120 °C to -60 °C at 5 °C/min. The heating cycle began after holding the SMA for 1.0 minute at -60 °C. The SMA was then heated from -60 °C to 120 °C. Figure 2 shows the DSC test results of the SMA strip.

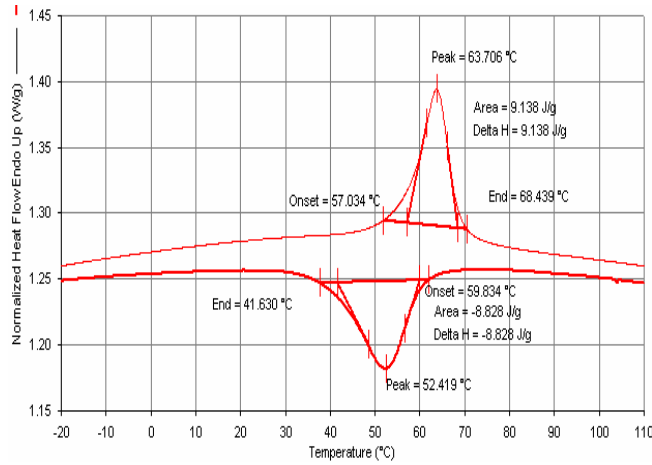


Figure 2. Transformation temperatures and latent heats (DSC Test).

Carnot Efficiency

The proportion of the Carnot efficiency that can be usefully realized in practical engines is typically 60 %. Once the design of an engine has been optimized, the only way to get higher performance is by increasing the Carnot efficiency or by extension of the difference in temperatures of sources of heat between which the engine operates. The Carnot efficiency of SMA heat engine is [15][19]

$$\eta_{Car} = \frac{A^f(\sigma_{max}) - M^f(\sigma \rightarrow 0)}{A^f(\sigma_{max})} \quad (1)$$

$$A^f(\sigma) = A^{of} + \sigma \frac{dA^f}{d\sigma} \quad (2)$$

Where $\frac{dA^f}{d\sigma}$ is the slope in stress-temperature diagram of the SMA strip. Hence,

$$\eta_{Car} = 1 - \frac{M^f(\sigma \rightarrow 0)}{A^{of} + \sigma_{max} \frac{dA^f(\sigma)}{d\sigma}} \quad (3)$$

Theoretically, $M^f(\sigma \rightarrow 0)$ at zero stress and M^{of} should be the same value [17]. Hence the Carnot efficiency is like that,

$$\eta_{Car} = 1 - \frac{M^{of}}{A^{of} + \sigma_{max} \frac{dA^f(\sigma)}{d\sigma}} = 15.3 \% \quad (4)$$

Substituting into equation (4) the values of the transformation temperature getting from the DSC test, $dA^f/d\sigma = 1/6.7 \text{ }^\circ\text{K/M Pa}$ [20] and 200 M Pa stress. Then the Carnot efficiency is 15.3 %. The energy efficiency is theoretically restricted by the Carnot efficiency since an SMA actuator is a heat engine operating at low temperature.

Thermal Efficiency of Ideal SMA Heat Engine

The thermal efficiencies of SME heat engines, which are of interest, have been estimated from thermodynamic magnitudes (enthalpies) and the transformation temperatures of the alloys [16]. The thermal efficiency for the ideal shape memory heat engine cycle is given [16][17] as

$$\eta_{in} = \frac{\Delta H \times \Delta T_o}{T_o \times (C_p \times \Delta T_o + \Delta H(\sigma))} \quad (5)$$

Where C_p is the specific heat of the material and $\Delta T_o = T_o(\sigma) - T_o$. Also ΔH (latent heat) in the denominator of the efficiency equation is a function of stress,

$$\Delta H(\sigma) = \Delta H \times T_o(\sigma) / T_o \quad (6)$$

T_o is estimated as

$$T_o = 1/2 \times (M^{os} + A^{os}), \text{ or } 1/2 \times (M^{of} + A^{of}) \quad (7)$$

To calculate $T_o(\sigma)$, we take

$$\begin{aligned} T_o(\sigma) &= 1/2 \times [M^s(\sigma) + A^s(\sigma)] \\ &= 1/2 \times [M^{os} + (dM^s/d\sigma) \times \sigma + A^{os} + (dA^s/d\sigma) \times \sigma] \\ &= T_o + (dM^s/d\sigma) \times \sigma \end{aligned} \quad (8)$$

The thermal efficiency can be obtain by utilizing DSC test data and $d\sigma/dT = 6.7$ M Pa [20] of the K-alloy. $d\sigma/dT = d\sigma/dM^s = d\sigma/dA^s$ is assumed to get T_o . Also the value of σ is assumed as 200 M Pa. Hence the thermal efficiency for the ideal shape memory heat engine cycle can be obtained from equation (5) as,

$$\eta_{th} = \frac{\Delta H \times \Delta T_o}{T_o \times (C_p \times \Delta T_o + \Delta H(\sigma))} = 3.12 \%$$

Where the value of C_p is 550 J/kg °K [17].

Gil and Planell [17] calculated the thermal efficiency of the NiTiCu shape memory alloys by means of calorimetric techniques and mechanical tests. Thermal efficiencies ranged from 4.7 % to 5.3 %. Generally efficiency of the SMA alloys is low compared to conventional heat engines. But the use of Shape Memory Alloy actuator can reduce the size, weight and complexity of the systems. Its power density is remarkable high such as 100 W/kg or more [21]. The conventional actuators produce a significant amount of noise, while the SMA actuator is completely silent. Thus, SMA actuators can be ideal for cases, such as robotic, micro/miniature and medical applications, where power density, simplicity of mechanism and silent actuation is more important than energy efficiency of the system.

The thermal efficiencies of three systems are shown in table 3. These values are very reasonable considering the 3.12 % of the ideal heat engine efficiency. The battery system efficiencies show much higher values than those of other systems due to its high efficiency in converting electrical energy to thermal energy and less additional power requirements. In implementation of these systems, the efficiency should be lower than the value of the table 3 due to additional energy losses and additional power requirements.

3. NUMERICAL ANALYSIS OF THE SMA ACTUATOR

3.1 Numerical Heat Transfer Analysis of SMA Actuator

To estimate the period of the heating and cooling cycle, and thus actuation frequency, a numerical heat transfer analysis of the SMA actuator was carried out with commercial software packages. The energy balance equation of the SMA strip can be written as:

$$\frac{\partial}{\partial t} [\rho_s C_p^o T_s + \rho_s \Delta H] dV = \frac{\partial}{\partial z} \left(k_s \frac{\partial T_s}{\partial z} \right) dV + q_{in} dA_{in} - q_{out} dA_{out} + q_{gen} dV \quad (9)$$

with temperature T , thermal conductivity k , density ρ , specific heat of the SMA strip C_p , time t and latent heat ΔH (J/g). The subscript s means SMA strip. Where q_{in} is energy input rate from the hot fluid, q_{out} is energy loss rate from the strip to environment and q_{gen} represents energy generation rate per volume. The SMA strip is heated by only convection heating. Therefore, there are no q_{out} and q_{gen} terms. In the phase transformation of an SMA, heat is absorbed during the reverse transformation (martensite to austenite) and it is released during the forward transformation (austenite to martensite). This heat is called the latent heat of transformation (ΔH). This latent heat is expressed by a variation with temperature of the redefined specific heat of the SMA C_p^* . The area under the curve described by the specific heat is the latent heat of transformation. During phase transformation the heating and the cooling of the SMA are slowed down due to the latent heat of transformation. When doing a transient heat transfer analysis it is therefore important to account this effect. An empirical relation describing the dependence of the specific heat with temperature is given in [5]. The certain transformation temperatures, latent heat and specific heat capacity, such as $A^f = 363.83$ °K and $A^s = 352.42$ °K at the values of 150 M Pa stress, were utilized in the followings equations.

For the forward transformation it is:

$$Cp_s^* = Cp_s^o + \Delta H \frac{\ln(100)}{|M^s - M^f|} e^{\frac{2\ln(100)}{|M^s - M^f|} \left| T - \frac{M^s + M^f}{2} \right|} \quad (10)$$

$$M^f < T < M^s$$

For the reverse transformation it is:

$$Cp_s^* = Cp_s^o + \Delta H \frac{\ln(100)}{|A^s - A^f|} e^{\frac{2\ln(100)}{|A^s - A^f|} \left| T - \frac{A^s + A^f}{2} \right|} \quad (11)$$

$$A^f < T < A^s$$

The original specific heat value of the SMA: Cp_s^o is 550 J/Kg °K [17]. The curves obtained for the variation of the specific heat of the SMA with temperature during the forward and reverse transformations at 150 M Pa stress are shown on figure 3.

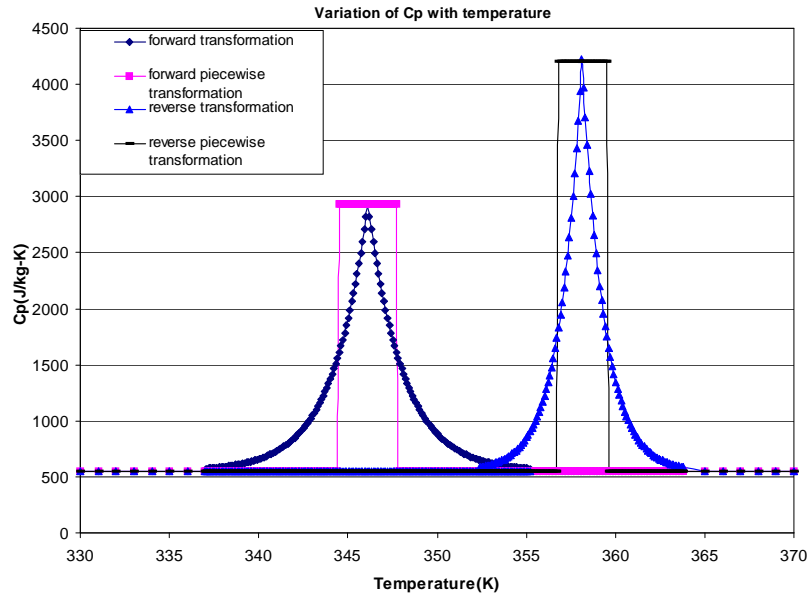


Figure 3. Variation of Cp with temperature.

For the numerical calculation, the FLUENT 5.5 and GAMBIT 1.3.0 commercial packages were used. The initial condition was $T=T_0$ (335 °K) and the boundary conditions for the inlet velocity and temperature of the fluid were 1 m/sec and 370 °K, respectively. For heating medium and cooling medium, water was selected. The flow is turbulent flow (Red = 3,630) and the standard k- ϵ model with two-layer zonal model for the near wall region was used. The circular channel wall was assumed to be an adiabatic boundary. Energy losses of both ends of channel were ignored. The circular channel and an SMA strip (12 mm x 0.9 mm) embedded in this channel ($D = 12$ mm, $L=200$ mm) is the computational domain shown in figure 4. The cross section of the domain is shown in figure 5. Half of the channel and strip were calculated by using symmetric conditions. The grid consists of about 200,400 computational cells for the calculation. This grid was generated by GAMBIT. The grid was denser near the SMA strip in order to capture the boundary layer.

The figure 3 shows a maximum increase of the value of the specific heat (Cp_s^*) of about 8 times of the original value. It was difficult to get FLUENT to run with the specific heat varying with temperature such as figure 3. Instead a piecewise variation has been adopted. The approximations used are shown on figure 3. The area under these approximations is the kept the same as the original, therefore conserving the value of the latent heat of transformation. However by conserving the same maximum value of specific heat during transformation, the transformation's start and finish temperatures had to be changed. The transformation is starting later and finishing earlier.

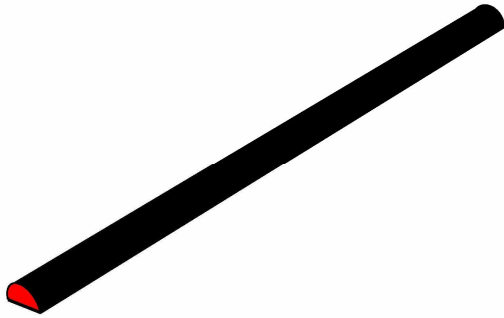


Figure 4. The computational domain.

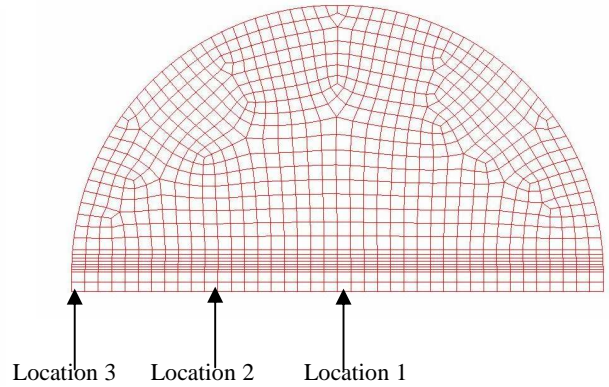
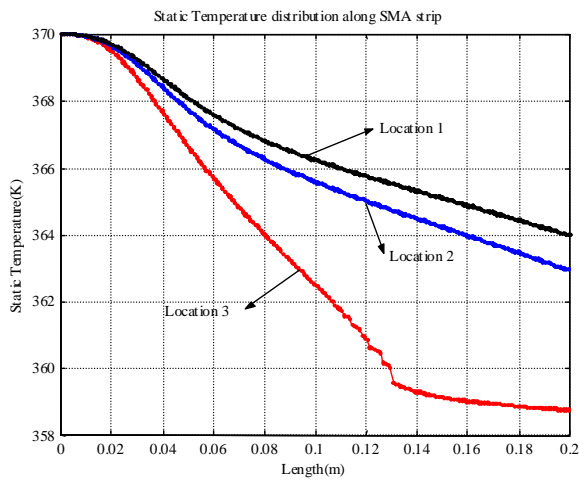


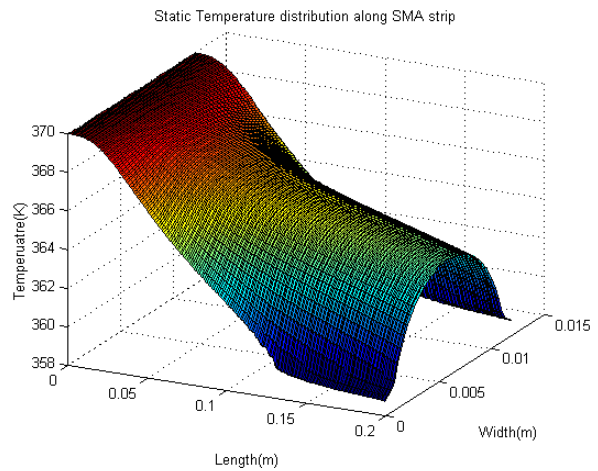
Figure 5. The computational grid.

3.2 Results of Numerical Analysis

The temperature calculation of the SMA strip is an unsteady heat transfer problem. The time step was 0.01 sec and maximum number of iterations for each time step was set at 200. The austenite finish temperature will be changed to around 360 °K from the 364 °K due to piecewise approximation of specific heat. The y^+ values at the wall were less than 5 except entrance region. This shows that the turbulent calculation was correctly done. After 1.3 sec, the temperature distribution along the strip was everywhere higher than 360 °K excluding corner of the strip, as shown in figure 6. The Figure 6 (a) shows temperature distribution along the length of the strip at three locations. The first is at the center of the strip (location 1 in figure 5), the third is the end of the strip (location 3), and the second is the middle line between the first and the third line (location 2). Figure 6 (b) shows temperature distribution of the whole strip. From the figure 5 and 6 the small amount of the strip still was in transformation ($M \rightarrow A$), but most region of the strip was fully transformed. After 0.9 sec, the temperature distribution along the strip without considering latent heat was above the 364 °K except the corner of the strip. The latent heat of strip should be considered in numerical calculation especially for the transient case in order to avoid overestimating heat transfer rate, thus actuation frequency. Cooling case was also calculated using room temperature water with 1 m/sec of velocity and 360 °K initial strip temperature. The cooling was faster than heating. Thus the actuation frequency was estimated around 0.5 Hz, even under high stress loading condition. Generally higher inlet velocity and higher inlet temperature increase the heat transfer rate to the SMA strip. The high boiling point fluids such as Ethylene Glycol can generate higher actuation frequency.



(a)



(b)

Figure 6. Temperature distribution along the SMA strip after 1.3 sec [FLUENT].

4. FUEL-POWERED COMPACT SMA ACTUATOR SYSTEM

4. First Design of Fuel-Powered Compact SMA Actuator System

From the comparison with other actuator systems in section 2, the fuel-powered SMA actuator system having the highest energy and power density was selected in order to develop compact SMA actuator system. To measure available force, displacement and actuation frequency, a fuel-powered SMA actuator system was designed. The actuator system is composed of a pump, valves, a combustor, an SMA element, a hot fluid tank, bellows and heat exchangers. The bellows used to prevent mixing between hot and cold fluid.

Figure 7 shows the first design of the fuel-powered SMA actuator system and the corresponding, its experimental setup. The load is applied constantly by dead weight for entire heating and cooling cycle. The strip was put through multiple thermal cycles by cycling its temperatures from the martensite finish temperature ($T < M^f$) to the austenite finish temperature ($T > A^f$) under a constant applied stress of 68 M Pa and 150 M Pa.

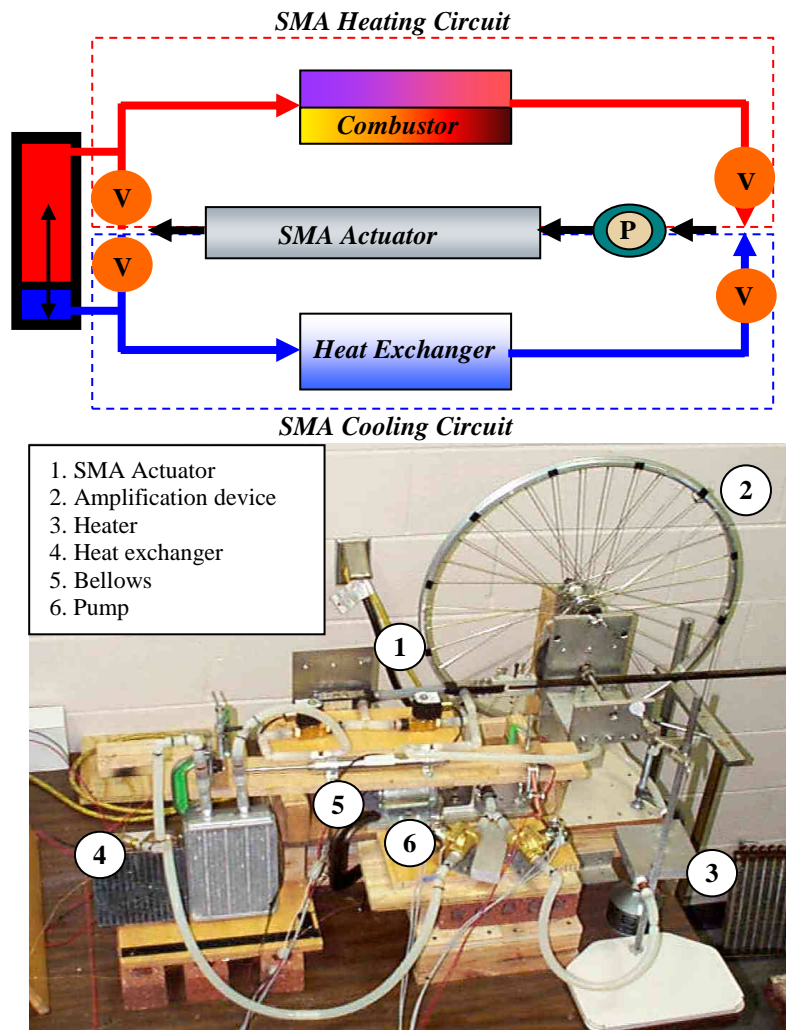


Figure 7. First Design of Fuel- Powered SMA Actuator System: Schematic of basic architecture (upper) and corresponding, its experimental setup (lower).

Figure 8 shows loading path during entire heating and cooling cycles. At the higher actuation frequency and under the higher stress condition, the strip can be in partial transformation due to the deduction of heating duration and the increase of transformation temperatures. The strain and displacement were measured with a LVDT.

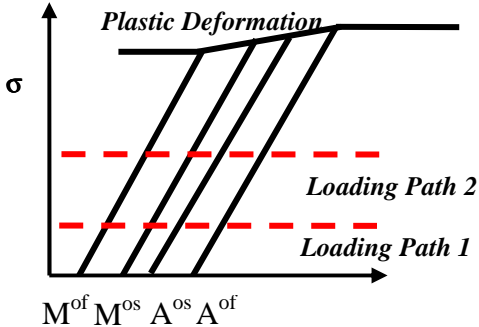


Figure 8. Heating and cooling cycle under constant applied stress.

4.2 Components of the SMA Actuator System

SMA Actuator

The SMA strip was embedded in a circular silicone tube, which is able to withstand high temperature and is able to bend and expand. The inside diameter of the tube is 12.7 mm and the wall thickness is 0.8 mm. Two steel connectors were utilized to hold the strip, as well as provide supply and return connections for the fluid flow and to transfer the actuation force to the mechanical stroke amplification device. The amplification mechanism increases the stroke by 86 times of initial strain of the strip and reduces the force by 82 times. Figure 10 shows the characteristics of the amplification device.



Figure 9. SMA Actuator with a circular silicone channel and connectors.

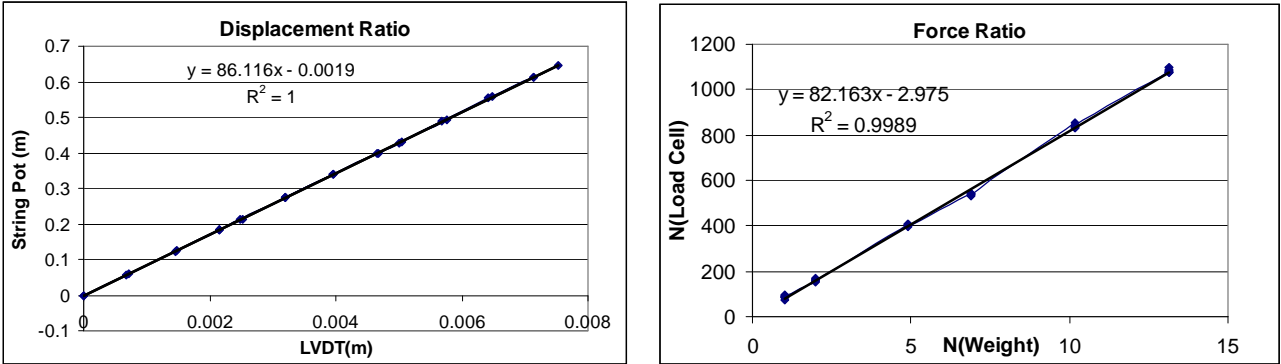


Figure 10. Performance characteristics of the amplification mechanism.

The SMA strip is K-alloy type, which is a Ni, Ti and Cu alloy and has 12 mm x 0.9 mm cross section area and 254 mm long including connections. Thus available length of the actuator is about 210 mm. Out of all the Shape Memory Alloys that have been discovered so far, Nickel-Titanium has proven to be the most flexible and beneficial in engineering applications. Ni-Ti Shape Memory Alloy has greater ductility, more recoverable motion, excellent corrosion resistance and stable transformation temperatures [22]. Copper can decrease hysteresis and lower the deformation stress (detwinning stress) of the martensite. The strip was annealed at 450 °C for 20 minutes. The transformation temperatures of the strip were obtained by DSC tests after annealing. This kind of SMA alloy has around 70 °C active A^f temperature and shows high-energy efficiency compared to other types of SMA alloys [16]. For the first actuator, one strip was utilized as the SMA element of the actuator.

Combustor and hot fluid tank

A 185gram compact commercial camping stove was utilized as the combustor. Its flame is adjustable up to 4000 watts and runs on a valved butane and propane mix cartridge, which contains 227 g of fuel. It can boil 1 liter of water within 3 minutes. A 127 mm x 127 mm x 25.4 mm hot fluid tank was fabricated by an aluminum block and has a 635 mm flow path inside of it. The aluminum block sealed by screws and RTV and was heated directly by the camping stove. Two K-type thermocouples were used to measure the temperature of hot fluid. The efficiency of this camping stove was estimated around 40 %.

Heat Exchanger

The cooling medium, after it removes the heat from the SMA strip goes through a heat exchanger where it disposes of that heat. For the first actuator system, two kinds of radiators with a 472 ml/sec fan were used. One is an automobile heater core and the other is a PC cooling radiator. It measures 152 mm x 178 mm x 5.1mm with a 870 Watt capacity.

Pump with Motor

The brass Omega FPUGR201 gear pump circulates heating and cooling media. Its maximum flow rate is 7.95 l/min at low pressure and can withstand 0.69 M Pa and 149°C. This pump circulates hot fluid and cold fluid alternatively. One pump system was selected to increase the energy density of the system. However, it suffers from some energy loss since hot and cold fluid heat and cool the gear pump itself. The pump was run by a DC motor. The pump runs constantly regardless of heating and cooling cycles. The solenoid valves control the heating and cooling medium circulated by the pump.

Solenoid valves

Four solenoid valves were utilized to control the heat and cooling circuits. The valves located before the pump in figure 4 were GC direct operated diaphragm 2 way solenoid valves. They can operated in pressure ranges from 0 Pa to 0.69 M Pa, up to 145 °C fluid temperature and have a Cv of 3.3. The other two valves were Parker 0.83 Cv direct acting valves. The operating pressure and temperature ranges are from 0 Pa to 0.138 M Pa and up to 85 °C, respectively. The GC valves are operated by on/off signal coming from controller while other two valves are controlled by bellows and switches.

Bellows

The mixing between hot and cold media must be avoided to reduce energy losses. A bellows was utilized to prevent mixing between hot and cold fluid caused by sharing common flow paths such as actuator channel and the volume inside the pump. Also, it can generate some kinds of force to aid in the fluid media circulation. A 152 mm stroke, double acting double rods American air cylinder was used as a bellows. For the first actuator system, the bellows and switches controlled two solenoid valves, which are located downstream of the SMA actuator (figure 4). An SR latch switch algorithm was utilized.

Control and Data acquisition

The data acquisition board used was a National Instrument AT-MIO-16XE-50. The board has 16 bit resolution and eight differential inputs. Two digital channels were used for the switches, three differential channels for thermocouples and the LVDT. A HP6268B DC power supply provided the power to the system. A power splitter board was controlled through a National Instrument PCI-6704 D/A board. The power splitter board takes the single input from the HP 6268B

power supply and splits it into six individually controlled channels, which are used to supply controlled power to motor and the solenoid valves. A Lab-windows program was put together to control the hardware and acquire data.

5. EXPERIMENTAL RESULTS AND DISCUSSIONS

Water was selected as heating and cooling medium from the numerical results because it was easy to handle and the boiling temperature of water is high enough to heat and cool the SMA strip around 0.5 Hz under high stress (150 MPa). The inlet velocity and inlet temperature were also determined based on numerical analysis. The volume flow rate of hot water and cold water was set as 0.11 l/sec by adjusting the power of the pump, thus the flow velocity inside the channel was around 1 m/sec. The actuator system was tested under 735 N constant load. Figure 11 shows the displacement of the strip under 735 N load for the close loop system. The hot water, after heating the SMA strip, returned back to the heater, which added enough energy to the hot water to compensate for its energy loss due to heating of SMA strip and other energy dissipations. The cold water, after cooling the SMA strip, returned back to the radiator where the thermal energy removed from SMA strip was dissipated to the surroundings by air forced convection.

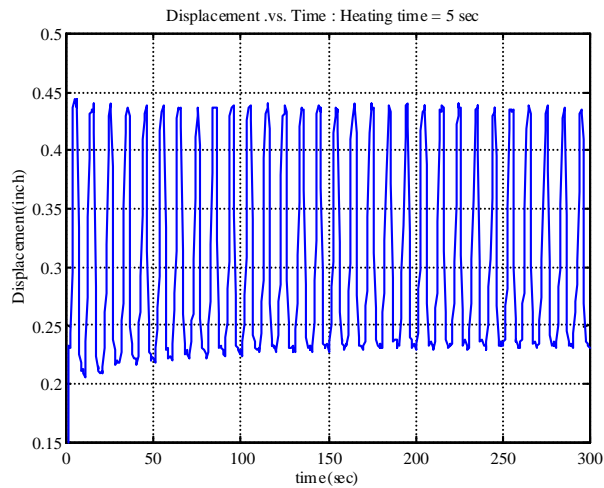


Figure 11. Strain Vs. Time under 735 N for the close loop system.

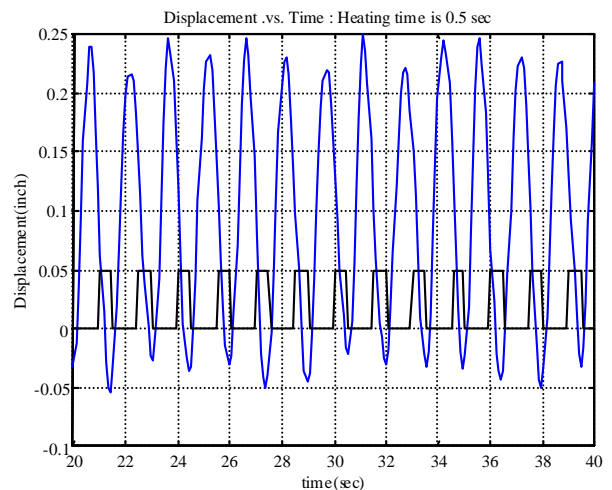


Figure 12. Strain Vs. Time under 735 N for the open loop system.

The 2.5 % strain and 0.1 Hz (heating time: 5 sec & cooling time: 5 sec) actuation frequency was obtained from the close loop system test. This result shows lower strain and slower frequency compared to the open loop system, in which the hot and cold water was not re-circulated in the system. The figure 12 and 13 show the results for the open loop system. The SMA actuator system can generate enough recovery stress and strain at 0.5 Hz actuation frequency. Figure 12 shows higher frequency under 735N than that of Figure 13 under 1560 N. The maximum operating pressure of the close loop system is about 69 K Pa in the heating (hot fluid) circuit. Pressure losses of the system and water vapor caused this pressure.

In the open loop test, actuation frequency of the SMA actuator (K-alloy, 12 mm x 0.9 mm) can be raised to 1 Hz (heating and cooling cycle) under 68 MPa load (735 N), and up to 0.5 Hz under 150 MPa load (1560 N). At least 3 % strain can be obtained by utilizing hot water (370 °K) and cold water (295 °K).

The lower strain and slower actuation frequency in the close loop system was mainly due to the mixing between hot and cold fluid in the system. As the number of cycles increases, the energy loss caused by the mixing increases. The cylinder and pump are also heat loss devices because they contain heating and cooling medium alternatively. Hence the hot fluid temperature goes down and the cold fluid temperature goes up. This degrades the performance of the heating and cooling circuit. More powerful heater and heat exchanger can overcome this mixing, but in that case the system might lose compactness and high energy density. One of the methods to prevent mixing is to adjust stroke length of the cylinder (bellows), thus making the channel volume and volume of other sharing passages equal to the volume of

bellows. If the mixing and energy loss were prevented properly, at least 0.5 Hz actuation frequency and 3 % recovery strain could be obtained.

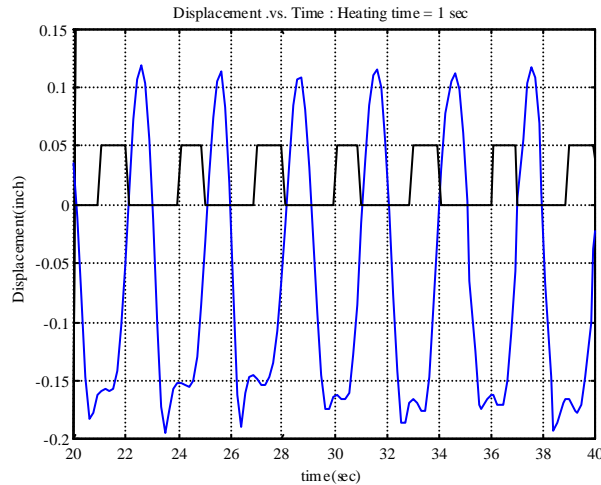


Figure 13. Strain Vs. Time under 1560 N for the open loop system.

The heating period of experimental results under high stress condition and 3 % recovery strain was around 1.0 sec in the open loop test. This shows somewhat faster than that of the numerical results, which show the heating period around 1.3 sec at 150 M Pa stress considering latent heat of the transformation. The partial transformation of the strip in experimental test and uncertainty of the material properties might cause this difference. The two-way trained wire can result in 4 % recovery stress when it is fully transformed [20]. The experimental results show 3 % recovery strain. The strip might be under partial transformation due to high stress condition and relatively high actuation frequency. Additional test for the properties of SMA strip such as specific heat needs in order to increase the accuracy of the numerical analysis. Thus the numerical results are reasonable considering partial transformation of the strip and uncertainty in properties of SMA strip. As mentioned above, the 0.5 Hz actuation frequency under 150 M Pa stress is obtained from the experimental test. This value shows good agreement with the prediction in section 3.

6. CONCLUSIONS

The fuel-powered SMA actuator system is simple and compact potentially compared to other actuator systems. The comparisons show that this system has much higher energy and power density than that of the battery and the fuel cell powered SMA actuator systems. The forced convection heating and cooling generated relatively high actuation frequency compared to resistive heating and air forced convection cooling. The results of the numerical heat transfer analysis are useful and reasonable compared to the results of the experimental test. Thus, in designing of the thermal induced SMA actuator, the transient heat transfer analysis with latent heat must be carried out and confirmed numerically to determine the design parameters and operating conditions. The fuel powered actuator system is being developed and modified to get high force actuation under relatively high actuation frequency. The first designed SMA actuator system could actuate the SMA strip (12mm x 0.9mm x 254 mm) at 0.5 Hz under 150 M pa stress with 3 % strain. This frequency is fairly high considering the size of strip. Fuel such as butane and propane is relatively cheap, easy to handle and easy to store in compact modules like gas cartridges. Hence the operating cost of this actuator system will be lower compared to batteries and fuel cells. This research also shows the energy savings that SMAs present us with, in systems where parasitic heat is already present. Heating of the SMA by utilizing existing parasitic heat in the vehicle/plant, this will yield a high energy density actuator.

We are focusing on optimization and miniaturization of the actuator system in order to increase power and energy density. A special combustor, valves, a pump and heat exchanger are being designed to develop the highly compact actuator system. The microchannel technology will be used to increase heat transfer rate, efficiency and compactness of the combustor and heat exchanger. The next design of compact actuator system will be designed to be modular in order to allow for alternative energy sources such as batteries, fuel cell and parasite heat. The energy density and power

density of the SMA actuator system will be measured at the next design of compact actuator system. Actuator fatigue test will be required to determine the life of the actuator as a function of actuation stress, strain and frequency. Test with high boiling point fluids such as Ethylene Glycol will be performed to get high actuation frequency and to increase energy density of the system.

7. ACKNOWLEDGMENTS

The authors would like to acknowledge the financial support of DARPA through the ARO Grant No DAAD19-01-0804. The authors would also like to thank Dr. Gary Anderson for his support and technical interest in this research.

8. REFERENCES

1. Johnson, A.D, "Nitinol Heat Engines", Intersociety Energy Conversion Engineering Conference Proceedings, pp530-534, 1975.
2. William S. Ginell, Joseph L. McNichols, Jr, and John S.Cary, "Nitinol Heat Engines for low-grade thermal energy conversion", Mechanical Engineering, pp28-33, 1979.
3. Zurab Saralidze, "Design and Creation of Heat Engines Working on the Basis of Phase Transformations in Solids and Using Nontraditional Sources of Heat Energy", Institute of Physics Georgian Academy of Sciences, Tbilisi Georgia, 2001.
4. Boyd, J. G and Lagoudas, D.C. "Thermomechanical response of shape memory composites", J. Intell. Mater. Struct 5, pp336-346, 1994.
5. A. Bhattacharyya, D.C. Lagoudas, Y wang and V.K. Kinra, "On the role of thermoelectric heat transfer in the design of SMA actuators; theoretical modeling and experiment", Smart Mater. Struct 4, pp252-263, 1995.
6. K.P. Brooks, C.J. Call, M. K. Drost, "Integrated Microchannel Combustor/Evaporator Development", ASME IMECE Conference, Nashville, TN, 1999.
7. Chad Harris, Mircea Despa, and Kevin Kelly, "Design and Fabrication of a Cross Flow Micro Heat Exchanger", Journal of Microelectromechanical Systems, Vol 9, No 4, pp502-508, 2000.
8. Rediniotis, O.K., Lagoudas, D.C., Garner, L. and Wilson, N. (1998) "Experiments and Analysis of an Active Hydrofoil with SMA Actuators," AIAA Paper No. 98-0102, 36th AIAA Aerospace Sciences Meeting, Reno, Nevada, January 1998.
9. Webb, G., Wilson, L., Lagoudas, D.C. and Rediniotis, O.K., "Adaptive Control of Shape Memory Alloy Actuators for Underwater Biomimetic Applications," AIAA Journal, Vol. 37, No.12, Dec. 1999.
10. Rediniotis, O. K., Lagoudas, D. C. and Wilson, L.N. (2000) "Development of a Shape Memory Alloy Actuated Underwater Biomimetic Vehicle," AIAA Paper No. 2000-0522, 38th Aerospace Science Meeting and Exhibit, January 2000, Reno, Nevada.
11. Bruce Lin "Conceptual design and modeling of hydrogen fuel cell scooters for urban aisa", Master thesis, Mechanical & Aerospace Engineering Department of Princeton University, Sept. 1999.
12. "Fuel cell power system for underwater vehicle", <http://www.fuelcell.kosone.com>.
13. "Generic battery Technology comparison", <http://www.madkatz.com>.
14. "Energy Density", <http://www.jrc.es/iptsreport/vol36/english/arte5en.gif>, In. J. Hydrogen energy, Sept. 1996.
15. D.C. Lagoudas and A. Bhattacharyya, "Modeling of Thin Layer Extensional Thermoelectric SMA Actuators", In. J.Solids Structures, Vol. 35, pp.331-362, 1998
16. A.P. Jardine, "Calorimetric techniques for the evaluation of thermal efficiencies of shape memory alloys", Journal of Materials Science, 24, pp.2587-2593, 1989.
17. F.J. Gil, J.A. Planell, "Thermal efficiencies of NiTiCu shape memory alloys", Thermochimica Acta 327, pp.151-154, 1999.
18. A.P. Jardine, "Calorimetric measurements of transformation thermodynamics and thermal efficiencies of NiTi helices", Journal of Materials Science, 23, pp.3314-3320, 1988.
19. B. Cunningham and K.H.G. Ashbee, "MARMEM ENGINES", Acta Metallurgica, Vol. 25, pp.1315-1321, 1977.
20. David A. Miller and Dimitris C. Lagoudas, "Thermo-Mechanical characterization of NiTiCu and NiTi SMA Actuators: Influence of plastic strains" Smart Material and Structures, 2000.
21. Koji Ikuta, "Micro/Miniature shape memory alloy actuator", IEEE, pp. 2156-2161, 1990.
22. Waram, T, "Actuator Design using Shape Memory Alloys", 2nd Edition.